APPLICATIONS OF SLIDING MODE CONTROL TO BENCHMARK PROBLEMS

J. C. Wu[1], J. N. Yang[2] and A. K. Agrawal[2]

[1] Currently, Assistant Professor, Dept. of Civil Engrg., Tamkang University, Taipei, Taiwan.

[2] Professor and Research Assistant, respectively, Dept. of Civil and Environmental Engineering, University of California, Irvine, CA 92697.

SUMMARY

In this paper, both the methods of continuous sliding mode control (*CSMC*) and continuous sliding mode control with compensators (*CSMC&C*) have been applied to two benchmark structures; namely, a building model equipped with an active mass driver system, and a building model equipped with an active tendon system. The *CSMC&C* strategy is a modification of *CSMC* to facilitate the design of static output feedback controllers and to provide a systematic tuning of the control effort. Due to the structural identification scheme used in the benchmark problems, in which the state variables are fictitious, one can not take the full advantages of static output feedback controllers. As a result, an observer is used in *CSMC* whereas a low-pass filter is incorporated for each measurement in *CSMC&C*. The purpose of using low-pass filters in *CSMC&C* is to transform the benchmark problems into strictly proper systems. The main advantage of the *CSMC&C* method is that the on-line computational effort is reduced since the dimension of filters and compensator is much smaller than that of an observer. Simulation results based on the *CSMC* and *CSMC&C* methods are presented and compared with that of the *LQG* method. Robustness of stability and noise rejection for each controller design are also illustrated by examining the loop transfer function. Simulation results for the benchmark problems indicate that the control performances for *LQG*, *CSMC* and *CSMC&C* are quite comparable.

KEYWORDS : Sliding Mode Control, Compensator, Benchmark Problem, Active Driver System, Active Tendon System, Low-Pass Filter

I. INTRODUCTION

The theory of sliding mode control (*SMC*) or variable structure system (*VSS*) was developed for robust control of uncertain nonlinear systems [e.g., Utkin[1], Zhou and Fisher[2]]. Its main idea is to design a controller to drive the response trajectory into the sliding surface, in which the motion of the system is stable. Applications of continuous sliding mode control (*CSMC*) that does not have chattering effect to the following seismic-excited structures have been studied: (i) linear and nonlinear or hysteretic buildings [Yang et al[3, 4, 5], Singh et al[6]], (ii) sliding-isolated buildings [Yang et al[7]], and (iii) parametric control, such as the use of active variable dampers (AVD) on bridges [Yang et al[8]] and active variable stiffness (AVS) systems [Yang et al[9]]. In addition to full-state feedback controllers, static output feedback controllers using only a limited number of sensors installed at strategic locations were also presented in the studies above. Shaking table experimental verifications of the *CSMC* methods for linear and sliding-isolated building models have been conducted [Yang et al[7, 10]]. Based on the simulations and experimental results, it was demonstrated that the continuous sliding mode control methods are robust and their performances are quite remarkable.

Recently, a technique for designing sliding mode controllers by introducing a fixed-order compensator has been presented [Yallapragada et al[11], Yang et al[12, 13]], referred to as *CSMC&C*. The main advantages of using a fixed-order compensator in sliding mode control are as follows: (i) the static output feedback controller can be designed easily using the theory of Linear Quadratic Regulator (*LQR*) static output feedback design, and (ii) the modulation of the response quantities and control efforts can be made in a systematic manner.

In this paper, both the methods of *CSMC* and *CSMC&C* are applied to two benchmark problems [Spencer et al[14, 15]] for the evaluation of their performances. For these two benchmark problems, the entire structure-control system is represented by the evaluation model from which the control performance is evaluated. The reduced-order model (or design model) with a smaller dimension is constructed for the controller design in order to reduce the time delay for on-line integration for dynamic output feedback controllers. Due to the identification scheme used in these two benchmark problems, the state variables are fictitious variables rather than the physical variables, such as displacements, velocities or accelerations. This excludes the applications and advantages of static output feedback controllers for *CSMC* and *CSMC&C*, since fictitious

variables can not be measured directly. Consequently, the dynamic output feedback controllers with on-line integration are used, and modifications have been made for *CSMC* and *CSMC&C*. For the *CSMC* method, an observer that is the modification of the Kalman-Bucy filter is implemented to estimate the state variables of the design model for computing the control command. For the *CSMC&C* method, a first-order low-pass filter is introduced for each feedback measurement to facilitate the dynamic output feedback design. Simulation results based on *CSMC* and *CSMC&C* are presented and their performances are compared with that of the *LQG* method. Since the control robustness for the stability and noise rejection for each controller design can be guaranteed by limiting the magnitude of the loop transfer function in the high frequency range, the plots of loop transfer functions for three control strategies are also presented for comparison.

II. FORMULATION

For the benchmark problems, the interactions among the structure, control devices, and earthquake were taken into account in the input-output relations, and the system dynamics is represented by the plant **P(s)** as shown schematically in Fig. 1. The controlled plant has two inputs, i. e., the earthquake $\ddot{x}_g$ and the actuator command u, and two outputs i. e., the control output **z** and measured output **y**. The control output, consisting of response variables of the structure and control devices, is adjusted for the control objective. The measured output, consisting direct measurements from the sensors, is used as the feedback quantities of control. The evaluation model given by [Spencer et al[14, 15]] is expressed as

$$\dot{\mathbf{x}} = \mathbf{A}\,\mathbf{x} + \mathbf{B}\,u + \mathbf{E}\,\ddot{x}_g \tag{1}$$

in which **x** is the state vector consisting 28 state variables for the active driver system (or 20 state variables for the active tendon system); u is a scalar control command; and $\ddot{x}_g$ is the ground acceleration. The matrices **A**, **B** and **E** are system matrix, control location matrix and excitation influence vector, respectively. The l-dimensional control output **z** and m-dimensional measured output **y** are given by

$$\mathbf{z} = \mathbf{C}_z\,\mathbf{x} + \mathbf{D}_z\,u + \mathbf{F}_z\,\ddot{x}_g \tag{2}$$

and

$$\mathbf{y} = \mathbf{C}_y\,\mathbf{x} + \mathbf{D}_y\,u + \mathbf{F}_y\,\ddot{x}_g + \mathbf{v} \tag{3}$$

, respectively, in which $\mathbf{C}_z$, $\mathbf{D}_z$, $\mathbf{F}_z$, $\mathbf{C}_y$, $\mathbf{D}_y$ and $\mathbf{F}_y$ are matrices with appropriate dimensions and $\mathbf{v}$ is the measurement noise vector. Hence, the plant $\mathbf{P}(s)$ can be partitioned as

$$\mathbf{P}(s) = \begin{bmatrix} \mathbf{P}_{z\ddot{x}_g} & \mathbf{P}_{zu} \\ \mathbf{P}_{y\ddot{x}_g} & \mathbf{P}_{yu} \end{bmatrix} \tag{4}$$

where

$$\begin{aligned} &\mathbf{P}_{z\ddot{x}_g} = \mathbf{C}_z(s\mathbf{I} - \mathbf{A})^{-1}\mathbf{E} + \mathbf{F}_z\ ;\ \mathbf{P}_{zu} = \mathbf{C}_z(s\mathbf{I} - \mathbf{A})^{-1}\mathbf{B} + \mathbf{D}_z\ ; \\ &\mathbf{P}_{y\ddot{x}_g} = \mathbf{C}_y(s\mathbf{I} - \mathbf{A})^{-1}\mathbf{E} + \mathbf{F}_y\ ;\ \mathbf{P}_{yu} = \mathbf{C}_y(s\mathbf{I} - \mathbf{A})^{-1}\mathbf{B} + \mathbf{D}_y \end{aligned} \tag{5}$$

In Eqs. (2) and (3) , the control output $\mathbf{z}$ and measured output $\mathbf{y}$ consist of the following physical quantities: (i) for the active mass driver system : $\mathbf{z} = [\,x_1, x_2, x_3, x_m, \dot{x}_1, \dot{x}_2, \dot{x}_3, \dot{x}_m, \ddot{x}_{a1}, \ddot{x}_{a2}, \ddot{x}_{a3}, \ddot{x}_{am}\,]'$ or their combinations, and $\mathbf{y} = [\,x_m, \ddot{x}_{a1}, \ddot{x}_{a2}, \ddot{x}_{a3}, \ddot{x}_{am}, \ddot{x}_g\,]'$, in which x_i is the displacement of i^{th} floor relative to the ground, x_m is the displacement of the active mass driver relative to the 3rd floor, $\ddot{x}_{ai}$ is the absolute acceleration of the i^{th} floor, and $\ddot{x}_{am}$ is the absolute acceleration of the mass driver, and (ii) for the active tendon system : $\mathbf{z} = [x_1, x_2, x_3, x_p, \dot{x}_1, \dot{x}_2, \dot{x}_3, \dot{x}_p, \ddot{x}_{a1}, \ddot{x}_{a2}, \ddot{x}_{a3}, f\,]'$ or their combinations, and $\mathbf{y} = [\,x_p, \ddot{x}_{a1}, \ddot{x}_{a2}, \ddot{x}_{a3}, f, \ddot{x}_g\,]'$, in which x_p and $\dot{x}_p$ are the displacement and velocity of the actuator piston, and f is the tendon force. In the controller design, one has the freedom to choose appropriate control outputs and measured outputs from $\mathbf{z}$ and $\mathbf{y}$ given above, based on the control objective and the sensor installation. As a result, the matrices $\mathbf{C}_z$, $\mathbf{D}_z$, $\mathbf{F}_z$, $\mathbf{C}_y$, $\mathbf{D}_y$ and $\mathbf{F}_y$ should be modified appropriately to be consistent with $\mathbf{z}$ and $\mathbf{y}$ used.

With fictitious state variables, the controller can be designed such that the control command is computed on-line through dynamic output feedback that uses the measured output as feedback quantities. The transfer function of dynamic output feedback, $\mathbf{K}(s)$, is shown in Fig. 1. To avoid serious time delay, the dimension of dynamic output feedback equations is restricted not to exceed 12 states. Therefore, a reduced-order design model with a dimension of r ($r \le 12$) was constructed to provide a template for the controller design. In what follows, the vectors $\mathbf{x}_r$, $\mathbf{y}_r$, $\mathbf{z}_r$, $\mathbf{F}_{zr}$, $\mathbf{F}_{yr}$, $\mathbf{E}_r$ and matrices $\mathbf{A}_r$, $\mathbf{B}_r$, $\mathbf{C}_{zr}$, $\mathbf{D}_{zr}$, $\mathbf{C}_{yr}$, $\mathbf{D}_{yr}$, are used to represent the corresponding vectors and matrices in the design model.

(A) Continuous Sliding Mode Control (CSMC) Using an Observer

Design of Sliding Surface

The objective of *CSMC* is to design a controller to drive the state trajectory into a sliding surface (reaching condition) and maintain it there, whereas the sliding surface is designed to be stable [Utkin[1], Zhou and Fisher[2]]. The sliding surface is expressed as $S = \mathbf{P}\,\mathbf{x}_r = 0$, where S is a scalar (since u is a scalar), and $\mathbf{P}$ is a ($1 \times r$) constant matrix called sliding surface matrix. To restrict the response trajectory to the sliding surface (i. e. $S = 0$ and $\dot{S} = 0$), and to stabilize the motion on the sliding surface, the matrix $\mathbf{P}$ can be determined by minimizing the integral of a quadratic function

$$J = \int_0^\infty \mathbf{x}_r'(t)\ \mathbf{C}_{zr}'\ \mathbf{Q}\ \mathbf{C}_{zr}\ \mathbf{x}_r(t)\ \ dt \tag{6}$$

In Eq. (6), $\mathbf{Q}$ is an appropriate (l x l) positive semi-definite weighting matrix [Yang et al[3]].

Design of Controller for Reaching Condition

The stable controller is designed such that a non-positive time derivative of a Lyapunov function $V = 0.5\, S' S$ is ensured at every time instant, i. e., $\dot{V} \le 0$. The continuous sliding mode controller, in general, can be expressed as [Yang et al[3, 5]]

$$u = \mathbf{K}_b\,\mathbf{x}_r + K_f\,\ddot{x}_g \tag{7}$$

in which $\mathbf{K}_b$ is the feedback gain and K_f is the feedforward gain given, respectively, by

$$\mathbf{K}_b = -(\mathbf{P}\,\mathbf{B}_r)^{-1}\,\mathbf{P}\,\mathbf{A}_r - \delta\ \mathbf{B}_r'\,\mathbf{P}'\,\mathbf{P} \tag{8}$$

and

$$K_f = -(\mathbf{P}\,\mathbf{B}_r)^{-1}\,\mathbf{P}\,\mathbf{E}_r \tag{9}$$

in which δ is the gain margin (scalar). Since the first term in Eq. (7) is the state feedback, a stable observer will be designed independently to estimate the state $\mathbf{x}_r$ from the measured output $\mathbf{y}_r$ based on the separation theorem.

Design of Observer

First, we consider the case in which the feedforward compensation is ignored, i.e., $K_f = 0$. Assuming that the earthquake $\ddot{x}_g$ and the measurement noise $\mathbf{v}$ are uncorrelated Gaussian white noise processes, the well-known Kalman-Bucy filter can be modified as

$$\dot{\hat{\mathbf{x}}}_r = \mathbf{A}_r \hat{\mathbf{x}}_r + \mathbf{B}_r u + \mathbf{L}_o(\mathbf{y}_r - \mathbf{C}_{yr} \hat{\mathbf{x}}_r - \mathbf{D}_{yr} u) \tag{10}$$

in which $\hat{\mathbf{x}}_r$ is the estimate of the state. The observer gain matrix $\mathbf{L}_o$ in Eq. (10) is obtained as

$$\mathbf{L}_o = (\mathbf{P}_o \mathbf{C}'_{yr} + \mathbf{S}_o)\mathbf{R}_o^{-1} \tag{11}$$

where $\mathbf{P}_o$ is the solution of the Riccati matrix equation

$$\mathbf{P}_o \overline{\mathbf{A}} + \overline{\mathbf{A}}' \mathbf{P}_o - \mathbf{P}_o \mathbf{C}'_{yr} \mathbf{R}_o^{-1} \mathbf{C}_{yr} \mathbf{P}_o + \mathbf{Q}_o - \mathbf{S}_o \mathbf{R}_o^{-1} \mathbf{S}'_o = 0 \tag{12}$$

in which

$$\overline{\mathbf{A}} = \mathbf{A}'_r - \mathbf{C}'_{yr} \mathbf{R}_o^{-1} \mathbf{S}'_o \tag{13}$$

In Eqs.(11)-(13), $\mathbf{Q}_o$, $\mathbf{S}_o$ and $\mathbf{R}_o$ are the partitions of the auto-power spectral density matrix of the vector $\begin{bmatrix} \mathbf{E}'_r \ddot{x}_g & \mathbf{F}'_{yr} \ddot{x}_g + \mathbf{v}' \end{bmatrix}^T$, given by

$$\mathbf{Q}_o = \mathbf{E}_r S_{\ddot{x}_g \ddot{x}_g} \mathbf{E}'_r ; \quad \mathbf{S}_o = \mathbf{E}_r S_{\ddot{x}_g \ddot{x}_g} \mathbf{F}'_{yr} ; \quad \mathbf{R}_o = \mathbf{S}_{vv} + \mathbf{F}_{yr} S_{\ddot{x}_g \ddot{x}_g} \mathbf{F}'_{yr} \tag{14}$$

where $S_{\ddot{x}_g \ddot{x}_g}$ and $\mathbf{S}_{vv}$ are the power spectral densities of $\ddot{x}_g$ and $\mathbf{v}$, respectively.

With the feedback gain $\mathbf{K}_b$, the observer equation for on-line integration becomes

$$\dot{\hat{\mathbf{x}}}_r = (\mathbf{A}_r + \mathbf{B}_r \mathbf{K}_b - \mathbf{L}_o \mathbf{C}_{yr} - \mathbf{L}_o \mathbf{D}_{yr} \mathbf{K}_b) \hat{\mathbf{x}}_r + \mathbf{L}_o \mathbf{y}_r \tag{15}$$

In addition to their individual stability, the observer gain $\mathbf{L}_o$ and controller gain $\mathbf{K}_b$ should be designed to guarantee that $(\mathbf{A}_r + \mathbf{B}_r \mathbf{K}_b - \mathbf{L}_o \mathbf{C}_{yr} - \mathbf{L}_o \mathbf{D}_{yr} \mathbf{K}_b)$ is also stable. The control command in Eq. (7) at every sampling time instant is given by

$$u = \mathbf{K}_b \hat{\mathbf{x}}_r \tag{16}$$

and the $\mathbf{K}(s)$ matrix in the block diagram of Fig. 1 can be expressed as

$$\mathbf{K}(s) = \mathbf{K}_b (s\mathbf{I} - \mathbf{A}_r - \mathbf{B}_r \mathbf{K}_b + \mathbf{L}_o \mathbf{C}_{yr} + \mathbf{L}_o \mathbf{D}_{yr} \mathbf{K}_b)^{-1} \mathbf{L}_o \tag{17}$$

If the feedforward compensation K_f is included in the *CSMC* controller, the reduced-order design model can be expressed as

$$\dot{\mathbf{x}}_r = \mathbf{A}_r \mathbf{x}_r + \mathbf{B}_r u + \overline{\mathbf{E}}_r \ddot{x}_g \tag{18}$$

in which $\overline{\mathbf{E}}_r = \mathbf{E}_r + \mathbf{B}_r K_f$ and u involves only the feedback loop. Therefore, the design of the observer follows Eqs. (10)-(15) except that the parameters $\mathbf{Q}_o$ and $\mathbf{S}_o$ are modified as

$$\mathbf{Q}_o = \overline{\mathbf{E}}_r \mathbf{S}_{\ddot{x}_g \ddot{x}_g} \overline{\mathbf{E}}_r' ; \quad \mathbf{S}_o = \overline{\mathbf{E}}_r \mathbf{S}_{\ddot{x}_g \ddot{x}_g} \mathbf{F}_{yr}' \tag{19}$$

Hence, the resulting control command at every sampling time instant is given by

$$u = \mathbf{K}_b \hat{\mathbf{x}}_r + K_f \ddot{x}_g \tag{20}$$

(B) Continuous Sliding Mode Control with Compensator (CSMC&C)

For the design of *CSMC&C* controllers, instead of using an observer, a first-order filter is introduced for the measured output $\mathbf{y}_r$ as follows

$$\dot{\eta} = \mathbf{A}_\eta \eta + \mathbf{B}_\eta \mathbf{y}_r \tag{21}$$

where η represents the m-dimensional new output feedback vector; $\mathbf{A}_\eta$ and $\mathbf{B}_\eta$ are filter coefficient matrices. Combining Eq. (21) and the state equation of the design model, one obtains the $(r + m)$ augmented design model

$$\dot{\tilde{\mathbf{x}}}_r = \tilde{\mathbf{A}}_r \tilde{\mathbf{x}}_r + \tilde{\mathbf{B}}_r u + \tilde{\mathbf{E}}_r \tilde{\mathbf{W}} \tag{22}$$

where

$$\tilde{\mathbf{x}}_r = \begin{pmatrix} \mathbf{x}_r \\ \eta \end{pmatrix} ; \tilde{\mathbf{A}}_r = \begin{bmatrix} \mathbf{A}_r & 0 \\ \mathbf{B}_\eta \mathbf{C}_{yr} & \mathbf{A}_\eta \end{bmatrix} ; \tilde{\mathbf{B}}_r = \begin{pmatrix} \mathbf{B}_r \\ \mathbf{B}_\eta \mathbf{D}_{yr} \end{pmatrix} ; \tilde{\mathbf{E}}_r = \begin{pmatrix} \mathbf{E}_r & 0 \\ \mathbf{B}_\eta \mathbf{F}_{yr} & \mathbf{B}_\eta \end{pmatrix} ; \tilde{\mathbf{W}} = \begin{pmatrix} \ddot{x}_g \\ \mathbf{v} \end{pmatrix} \tag{23}$$

The control output $\mathbf{z}_r$ and the new measured output η for the augmented design model become

$$\mathbf{z}_r = \tilde{\mathbf{C}}_{zr} \tilde{\mathbf{x}}_r + \mathbf{D}_{zr} u + \mathbf{F}_{zr} \ddot{x}_g \tag{24}$$

and

$$\eta = \tilde{\mathbf{C}}_{yr} \tilde{\mathbf{x}}_r \tag{25}$$

where $\tilde{\mathbf{C}}_{zr} = [\, \mathbf{C}_{zr} \,,\, 0 \,]$ and $\tilde{\mathbf{C}}_{yr} = [\, 0 \,,\, \mathbf{I}_m \,]$ with I_m being an identity matrix of m dimension. Note that Eq. (25) has a strictly proper form. As observed from Eqs. (22)-(25), the introduction of η provides the controller with the flexibility to make trade-off among the control output $\mathbf{z}_r$, the feedback output η, and the control command u.

For the benchmark problems, the structural response is dominated by the lower frequency component and the system uncertainty is more significant at high frequency. It is beneficial to

weight more on the low frequency, and hence a low-pass filter is chosen such that the high frequency component in $\mathbf{y}_r$ is filtered out. For simplicity, the low-pass filter can be used independently for each measurement so that $\mathbf{A}_\eta$ and $\mathbf{B}_\eta$ are diagonal matrices with every diagonal element equal to a_i and b_i, respectively. One can further let $a_i = b_i$ such that the transfer function of the individual filter equation is $a_i/(s+a_i)$, where a_i is referred to as the roll-off frequency.

Design of Sliding Surface

Consider a 2-dimensional compensator with the state vector $\mathbf{q} = [\, q_1 \,,\, q_2 \,]'$ as shown in Fig. 2 [Yang et al[12, 13], Wu[16]],

$$\dot{q}_1 = L_{11}\, q_1 + L_{12}\, q_2 + \mathbf{N}_1\, \eta \tag{26}$$

$$\dot{q}_2 = L_{21}\, q_1 + L_{22}\, q_2 + \mathbf{N}_2\, \eta + D_2\, u + E_{12}\, \ddot{x}_g \tag{27}$$

in which $\mathbf{N}_1$, $\mathbf{N}_2$ are matrices with appropriate dimensions, and L_{11}, L_{12}, L_{21}, L_{22}, D_2 and E_{12} are scalars. If feedforward compensation is neglected, then E_{12} is zero. Otherwise, E_{12} is normally chosen to be the element of excitation vector corresponding to the controller location. The sliding surface is expressed in terms of the compensator variables q_1 and q_2 as

$$S = P_1\, q_1 + P_2\, q_2 = 0 \tag{28}$$

The sliding surface coefficients P_1 and P_2, and compensator coefficients, $\mathbf{N}_1$, $\mathbf{N}_2$, L_{11}, L_{12}, L_{21}, L_{22} and D_2, are determined by minimizing an objective function

$$J = \mathrm{E}\left[\, \int_0^\infty \bar{\mathbf{z}}_r'\, \mathbf{Q}_z\, \bar{\mathbf{z}}_r + \eta'\, \mathbf{Q}_\eta\, \eta + q_1\, Q_{q_1}\, q_1 + u_{eq}\, R_u\, u_{eq} + \dot{q}_1\, R_{\dot{q}_1}\, \dot{q}_1 \;\, dt \right] \tag{29}$$

in which $\bar{\mathbf{z}}_r = (\, \mathbf{C}_{zr}\, \mathbf{x}_r + \mathbf{D}_{zr}\, u_{eq})$ and u_{eq} is the equivalent control force. The detail derivations and design procedures will be described in the Appendix. After minimization, the equivalent control force can be computed by

$$u_{eq} = \mathbf{G}\, \eta + H\, q_1 \tag{30}$$

where $\mathbf{G}$ and H have been obtained in the process of minimization as described in the Appendix.

Design of Controller for Reaching Condition

The controller is designed such that the time derivative of a Lyapunov function $V = 0.5\, S'\, S$ is non-positive at every time instant, i.e., $\dot{V} \le 0$. The resulting *CSMC&C* controller is given by [Yang et al[12, 13], Wu[16]]

$$u = u_{eq} - [\, M_{c1} + (P_2\, D_2)^{-1}\, \delta\, P_1 \,]\, q_1 - [\, M_{c2} + (P_2\, D_2)^{-1}\, \delta\, P_2 \,]\, q_2 - D_2^{-1} E_{12}\, \ddot{x}_g \qquad (31)$$

in which

$$M_{c1} = (P_2\, D_2)^{-1}\, (\, P_1\, L_{12}\, P_2^{-1}\, P_1 + P_2\, L_{22}\, P_2^{-1}\, P_1) \qquad (32)$$

$$M_{c2} = (P_2\, D_2)^{-1}\, (P_1\, L_{12} + P_2\, L_{22}) \qquad (33)$$

and δ is the gain margin. The feedforward term, $-D_2^{-1}\, E_{12}\, \ddot{x}_g$, in Eq. (31) can be used to improve the control performance. The control command in Eq. (31) can be expressed in terms of the feedback loop and feedforward compensation as,

$$u = \mathbf{K_b} \begin{bmatrix} \eta \\ q_1 \\ q_2 \end{bmatrix} + K_f\, \ddot{x}_g \qquad (34)$$

where the feedback gain matrix, $\mathbf{K_b}$, and feedforward gain matrix, K_f, are given by

$$\mathbf{K_b} = [\mathbf{G} \;,\; H - M_{c1} - (P_2\, D_2)^{-1}\, \delta\, P_1 \;,\; -M_{c2} - (P_2\, D_2)^{-1}\, \delta\, P_2\,] \qquad (35)$$

$$K_f = -D_2^{-1}\, E_{12} \qquad (36)$$

Dynamic Output Feedback

As observed from Eq. (34), the feedback loop of the controller u involves the filter output vector η and the compensator variables q_1 and q_2, which should be computed on-line. Usually, if a hardware low-pass filter is implemented to each measurement, the output η of the filter is considered to be the direct measurement quantities. Then, η is used in Eqs.(26)-(27) to compute q_1 and q_2. In this case, the dynamic output feedback equation is the 2-dimensional compensator equation given in Eq. (26) and (27). Here, we assume that a software low-pass filter is used, therefore, the first-order filter, Eq. (21), and the compensator, Eqs. (26)-(27), form a system of dynamic output feedback equations with a (m+2)-dimensional state vector ξ,

$$\dot{\xi} = \mathbf{A}_\xi \xi + \mathbf{B}_\xi u + \mathbf{E}_\xi \mathbf{y}_r + \begin{bmatrix} 0 \\ 0 \\ E_{12} \end{bmatrix} \ddot{x}_g \tag{37}$$

where

$$\xi = \begin{bmatrix} \eta \\ q_1 \\ q_2 \end{bmatrix} ; \mathbf{A}_\xi = \begin{bmatrix} \mathbf{A}_\eta & 0 & 0 \\ \mathbf{N}_1 & L_{11} & L_{12} \\ \mathbf{N}_2 & L_{21} & L_{22} \end{bmatrix} ; \mathbf{B}_\xi = \begin{bmatrix} 0 \\ 0 \\ D_2 \end{bmatrix} ; \mathbf{E}_\xi = \begin{bmatrix} \mathbf{B}_\eta \\ 0 \\ 0 \end{bmatrix} \tag{38}$$

Substituting Eq.(34) into Eq. (37) , one obtains

$$\dot{\xi} = (\mathbf{A}_\xi + \mathbf{B}_\xi \mathbf{K}_b) \xi + \mathbf{E}_\xi \mathbf{y}_r \tag{39}$$

To maintain the stability of Eq. (39) for the on-line integration, the filter and compensator should be designed such that $(\mathbf{A}_\xi + \mathbf{B}_\xi \mathbf{K}_b)$ is stable. In the simulation for the control performance, $\mathbf{y}_r$ in Eq. (39) is the actual measurement from the sensors. As observed from Eq. (39), one advantage of the *CSMC&C* method is that it involves less on-line computational effort than the use of an observer in *CSMC* and *LQG* strategies.

Consequently, the $\mathbf{K}(s)$ matrix for *CSMC&C* in the block diagram of Fig. 1 can be expressed as

$$\mathbf{K}(s) = \mathbf{K}_b (s\mathbf{I} - \mathbf{A}_\xi - \mathbf{B}_\xi \mathbf{K}_b)^{-1} \mathbf{E}_\xi \tag{40}$$

(C) Control Robustness

While the performance of the controller is important, both the robustness of the control performance with respect to system uncertainties, noise and disturbance rejection, and the robustness of the structural stability with respect to system uncertainties are equally important. In particular, for civil engineering applications, uncertainties in damping, stiffness and excitation are quite significant and should be considered. When the control performance is evaluated by the measured output $\mathbf{y}$ and the system is matched (i. e., $\mathbf{E} = \mathbf{B}$), the robustness criterion for the control performance with respect to system uncertainty and disturbance is that the minimum singular value of $P_{yu}(i\omega)$ $K(i\omega)$ should be kept as large as possible in the low frequency range [see Doyle et al[17]]. For the robustness of control performance with respect to noise and the robustness of stability with respect to system uncertainties, the maximum singular value of

$P_{yu}(i\omega)$ $K(i\omega)$ should be as small as possible in the high frequency range [see Doyle et al[17]]. For the benchmark problems, the above criterion for the robustness of control performance with respect to system uncertainties and disturbances may not be applicable because our performance is based on **z** instead of **y** and the system is not matched. However, the criterion for examining the stability robustness and noise rejection is applicable.

Moreover, since the dimensions of $\mathbf{P}_{yu}(i\omega)$ and $\mathbf{K}(i\omega)$ are (mx1) and (1xm), respectively, the maximum singular value of $\mathbf{P}_{yu}(i\omega)$ $\mathbf{K}(i\omega)$ is equal to the singular value of $\mathbf{K}(i\omega)$ $\mathbf{P}_{yu}(i\omega)$ (a scalar), which is referred to as the loop transfer function of the controller. The plot of $\mathbf{K}(i\omega)$ $\mathbf{P}_{yu}(i\omega)$ in dB versus the frequency for each control design will be presented and compared with the specification of the stability robustness described in Spencer et al[14], i.e., -5dB for all frequencies above 35 Hz.

For *LQG* and *CSMC* controllers in which Kalman-Bucy filters are used as observers, a larger intensity $\mathbf{S}_{vv}$ of the measurement noise (or equivalently, a smaller intensity $S_{\ddot{x}_g\ddot{x}_g}$ of excitation) for the observer design will suppress the noise. Since the noise consists of high frequency components, the loop transfer function will be smaller in the high frequency range. In this case, however, the estimation of the state might be degraded. Therefore, a trade-off should be made for the choice of $\mathbf{S}_{vv}$. For *CSMC&C* controllers that use a first-order low-pass filter for the feedback measurements, the loop transfer function will be smaller in the high frequency range for smaller $\mathbf{A}_\eta$ and $\mathbf{B}_\eta$. This is because the effect of the measurement noise is less amplified.

III. NUMERICAL SIMULATION AND CONTROL PERFORMANCE

The performances of *CSMC* and *CSMC&C* algorithms for two benchmark problems will be demonstrated by numerical simulations using the MATLAB SIMULINK program for the evaluation model. The El Centro and Hachinohe earthquake records as well as an artificial earthquake with the nominal Kanai-Tajimi spectrum given in [Spencer et al[14, 15]] ($\omega_g = 37.3 \frac{\text{rads}}{\text{sec}}$, $\zeta_g = 0.3$, and $T_f = 300$ seconds for the AMD problem, and $\omega_g = 14.5 \frac{\text{rads}}{\text{sec}}$, $\zeta_g = 0.3$, and $T_f = 750$ seconds for the active tendon problem; for computational simplicity, no maximization over (ω_g, ζ_g) was performed) will be used for simulations. The simulation results based on the LQG control method are also presented for comparison.

Benchmark Problem No. 1: Active Mass Driver System

The response quantities of the active mass driver system with zero control input, are listed in Table 1. Peak response quantities under El Centro and Hachinohe earthquake records are shown in columns (2) and (3) of the upper part of Table 1, whereas the the temporal root-mean-square responses under the artificial earthquake, denoted by σ, are shown in column (5) of the upper part of Table 1.

With active control, the control output $\mathbf{z}_r$ is chosen to be $\mathbf{z}_r = [\, d_1, d_2, d_3, x_m, \dot{x}_1, \dot{x}_2, \dot{x}_3, \dot{x}_m, \ddot{x}_{a1}, \ddot{x}_{a2}, \ddot{x}_{a3}, \ddot{x}_{am} \,]'$ where d_i is the i^{th} interstory drift. With such a choice of $\mathbf{z}_r$, the vector $\mathbf{F}_{zr}$ and matrices $\mathbf{C}_{zr}$ and $\mathbf{D}_{zr}$ for the design model are different from those given in Spencer et al[14]. However, these can be obtained easily by a simple transformation. For each control strategy, three different design cases (output feedback) are considered; namely, 5-sensor, 3-sensor and 1-sensor. The measured output for these three cases are : (i) 5-sensor; $\mathbf{y}_r = [x_m, \ddot{x}_{a1}, \ddot{x}_{a2}, \ddot{x}_{a3}, \ddot{x}_{am}]'$, (ii) 3-sensor; $\mathbf{y}_r = [\ddot{x}_{a1}, \ddot{x}_{a2}, \ddot{x}_{a3}]'$, and (iii) 1-sensor; $\mathbf{y}_r = [\ddot{x}_{a3}]$. The (10x10) design model constructed by Spencer et al[14] was used for *LQG* controllers, whereas another (10x10) design model constructed by the 'balreal' and 'modred' functions in MATLAB CONTROL SYSTEM TOOLBOX was used for *CSMC* and *CSMC&C* controllers. The practical limitations, such as the maximum control command, maximum driver acceleration and maximum actuator stroke, and the simulation guidelines were given in Spencer et al[14]. All the controller are designed to utilize as much as possible the full capacity of the actuator without violating the constraints.

For the *LQG* controllers, the control output $\mathbf{z}_r$ and the control command u are tuned as follows: (i) 5-sensor case; $\mathbf{Q}$ = diag [130, 100, 100, 0, 0, 0, 0, 0, 1, 1, 10, 62], R = 50, (ii) 3-sensor case; $\mathbf{Q}$ = diag [32, 10, 10, 0, 0, 0, 0, 0, 1, 1, 1, 5], R = 13, and (iii) 1-sensor case; $\mathbf{Q}$ = diag [50, 43, 43, 0, 0, 0, 0, 0, 1, 1, 10, 12], R = 40. For the design of observers, $\gamma = S_{\ddot{x}_g \ddot{x}_g} / S_{v_i v_i} = 5$ is used. The controllers are designed such that the magnitude of the loop transfer function is below -5dB for frequencies above 35 Hz. As explained earlier, this can be achieved by use of a smaller γ ; however, a smaller γ may degrade the estimation of the state. After extensive simulations, a value γ =5 is used. The loop transfer functions, $\mathbf{K}(i\omega)\, \mathbf{P}_{yu}(i\omega)$, for the

LQG method are shown in Fig. 3 (a), in which the results for the 5-sensor, 3-sensor and 1-sensor cases are denoted by the solid curve, dashed-dot curve and dashed curve, respectively. J_1 to J_{10} for the evaluation model are presented in columns (2), (6) and (10) of Table 2 for 5-sensor, 3-sensor and 1-sensor cases, respectively. The root-mean-square command voltage under the stochastic earthquake is denoted by σ_u in Table 2, whereas the maximum command voltage under El Centro and Hachinohe earthquakes are denoted by $|u(t)|$ in Table 2. Under El Centro earthquake, the time history of the first-story drift, d_1, for the 5-sensor case are presented in Fig. 4 (a), in which the dotted curve and the solid curve represent the response quantity without control (zero control input) and that using *LQG* controller, respectively.

For *CSMC* controllers, the feedforward compensation is ignored for the fairness of comparisons. The design parameters for controllers are as follows: (i) 5-sensor case; $\mathbf{Q}$ = diag [1600, 1100, 1100, 0, 0, 0, 0, 110, 10, 15, 15, 1], δ = 40, (ii) 3-sensor case; $\mathbf{Q}$ = diag [1100, 1100, 1100, 0, 0, 0, 0, 165, 10, 15, 15, 1], δ = 40, and (iii) 1-sensor case; $\mathbf{Q}$ = diag [1500, 1100, 1100, 0, 10, 0, 0, 100, 10, 15, 15, 20], δ = 40. For the observer design, we choose $\gamma = S_{\ddot{x}_g\ddot{x}_g} / S_{v_i v_i} = 5$ such that the loop transfer function is smaller than -5dB for frequencies above 35 Hz. The loop transfer functions for the *CSMC* method are presented in Fig. 3 (b), in which the results for 5-sensor, 3-sensor and 1-sensor cases are denoted by the solid curve, dashed-dot curve and dashed curve, respectively. J_1 to J_{10} as well as σ_u and $|u(t)|$ for the evaluation model are presented in columns (3), (7) and (11) of Table 2 for 5-sensor, 3-sensor and 1-sensor cases, respectively. For the 5-sensor case using *CSMC* control, the time history of the first-story drift, d_1, under El Centro earthquake is presented in Fig. 4 (b) by the solid curve, whereas the dotted curve represents the corresponding response without control. The time history of the sliding surface S is plotted in Fig. 4 (c). As observed from Fig. 4 (c), the sliding surface $S = 0$ is not maintained because : (i) the feedforward compensation in Eq. (9) has been ignored, and (ii) the estimation of state $\mathbf{x}_r$ from an observer is required in the computation of the control command. However, the stability of S is always guaranteed.

The design parameters for *CSMC&C* controllers are as follows: (i) 5-sensor case; $\mathbf{A}_\eta = -7\,\mathbf{I}_5$, $\mathbf{B}_\eta = 7\,\mathbf{I}_5$, where $\mathbf{I}_m$ is an (mxm) identity matrix, $\mathbf{Q}_z$= diag [6000, 6000, 6000, 0, 0, 0, 0, 120, 1, 1, 1, 800], Q_{q_1} =1, $\mathbf{Q}_\eta$ = diag [0, 120, 120, 120, 0] , R_u= 0.1, $R_{\dot{q}_1}$ = 0.1, L_{12}= -1,

L_{22}= -0.001, P_1= 1, P_2= 1000, D_2= 1 and $\delta = 10^7$, (ii) 3-sensor case; $\mathbf{A}_\eta = -10\,\mathbf{I}_3$, $\mathbf{B}_\eta = 10\,\mathbf{I}_3$, $\mathbf{Q}_z$= diag [800, 800, 800, 0, 0, 0, 0, 50, 0, 0, 0, 60], $\mathbf{Q}_\eta$ = diag [100, 100, 100] and all other parameters are identical to case (i), and (iii) 1-sensor case; $\mathbf{A}_\eta = -10$, $\mathbf{B}_\eta = 10$, $\mathbf{Q}_z$= diag [6000, 700, 2000, 0, 0, 0, 0, 100, 0, 0, 0, 100], $\mathbf{Q}_\eta$ = 100 and all other parameters are identical to case (i). Note that the compensator coefficients $\mathbf{N}_1$, $\mathbf{N}_2$, L_{11} and L_{21} were computed from the design parameters above by minimizing Eq. (29) as presented in Appendix [also see Yang et al[12], Wu[16]]. For the fairness of comparisons, the feedforward part is ignored, i. e., E_{12} = 0. The choice of $\mathbf{A}_\eta$ and $\mathbf{B}_\eta$ depends on whether the requirement for the loop transfer function can be satisfied. As mentioned earlier, the requirement can be satisfied easily by choosing smaller $\mathbf{A}_\eta$ and $\mathbf{B}_\eta$. However, extensive simulation results indicate that it is difficult to adjust the control command to be more than 1 volt if smaller $\mathbf{A}_\eta$ and $\mathbf{B}_\eta$ are used. Therefore, a trade-off was made to choose the above values for $\mathbf{A}_\eta$ and $\mathbf{B}_\eta$. The loop transfer functions are plotted in Fig. 3 (c), in which the results for 5-sensor, 3-sensor and 1-sensor cases are denoted by the solid curve, dashed-dot curve and dashed curve, respectively. J_1 to J_{10} as well as σ_u and $|u(t)|$ for the evaluation model are presented in columns (4), (8) and (12) of Table 2. Note that we can not adjust the control command to be more than 1 volt for the 1-sensor case because of the limitation of such a configuration. For the 5-sensor case using *CSMC&C* control, the time history of the first-story drift under El Centro earthquake is presented in Fig. 4 (d) by the solid curve, whereas the dotted curve represents the response without control. The time history of the sliding surface S is plotted in Fig. 4 (e). As observed from Fig. 4 (e), the sliding surface motion S = 0 is well maintained, since the control command in Eq. (31) always guarantees $\dot{V} \le 0$.

As observed from Table 2, the control performances for three control methods, i.e., *LQG*, *CSMC* and *CSMC&C*, are quite comparable.

Benchmark Problem No. 2: Active Tendon System

The response quantities of the active tendon system with zero control command are listed in the lower part of Table 1. For active control, the control output $\mathbf{z}_r$ of the active tendon system is chosen as $\mathbf{z}_r = [d_1, d_2, d_3, x_p, \dot{x}_1, \dot{x}_2, \dot{x}_3, \dot{x}_p, \ddot{x}_{a1}, \ddot{x}_{a2}, \ddot{x}_{a3}, f\,]'$ in which d_i is the i^{th} interstory drift. For each control strategy, three different design cases are considered; namely, 5-sensor, 3-

sensor and 1-sensor. The measured output for these three cases are : (i) 5-sensor ; $\mathbf{y}_r = [x_p, \ddot{x}_{a1}, \ddot{x}_{a2}, \ddot{x}_{a3}, f]'$, (ii) 3-sensor ; $\mathbf{y}_r = [\ddot{x}_{a1}, \ddot{x}_{a2}, \ddot{x}_{a3}]'$ for *LQG* and *CSMC*, and $\mathbf{y}_r = [x_p, \ddot{x}_{a3}, f]'$ for *CSMC&C*, and (iii) 1-sensor ; $\mathbf{y}_r = [\ddot{x}_{a3}]$ for *LQG* and *CSMC*, and $\mathbf{y}_r = [f]$ for *CSMC&C*. A (12x12) design model constructed by the 'balreal' and 'modred' functions in MATLAB CONTROL SYSTEM TOOLBOX was used for *LQG* and *CSMC* controllers. Another (12x12) design model used for *CSMC&C* controllers is obtained by making a balanced transformation of the evaluation model and reducing the system by keeping the same eigen properties of the first 12 complex modes [Wu[16], Davison[18]]. The limitations, such as the maximum control command and actuator stroke, and the simulation guidelines were given in [Spencer et al[15]]. All the controller are designed to utilize as much as possible the full capacity of the actuator (i. e., control efforts) without violating the constraints.

For the *LQG* controllers, the control output $\mathbf{z}_r$ and the control command u are tuned as follows: (i) 5-sensor case; $\mathbf{Q}$ = diag [1, 1, 1, 0, 0, 0, 0, 0, 1, 1, 1, 6], $R = 4$, (ii) 3-sensor case; $\mathbf{Q}$ = diag [1, 1, 1, 0, 0, 0, 0, 0, 1, 1, 1, 6], $R = 4$, and (iii) 1-sensor case; $\mathbf{Q}$ = diag[1, 1, 1, 0, 0, 0, 0, 0, 1, 1, 1, 6], $R = 3$. For the observer, $\gamma = S_{\ddot{x}_g \ddot{x}_g} / S_{v_i v_i} = 0.5$ is used such that the magnitude of the loop transfer function is less than -5dB for frequencies above 35 Hz. The loop transfer functions, $\mathbf{K}(i\omega)\ \mathbf{P}_{yu}(i\omega)$, for the *LQG* method are shown in Fig. 5 (a), in which the 5-sensor, 3-sensor and 1-sensor cases are denoted by the solid curve, dashed-dot curve and dashed curve, respectively. J_1 to J_{10} as well as σ_u and $|u(t)|$ for the evaluation model are presented in columns (2), (6) and (10) of Table 3 for 5-sensor, 3-sensor and 1-sensor cases, respectively. For the 5-sensor case using *LQG* control, the time history of the third-story drift under El Centro earthquake is presented in Fig. 6 (a) by the solid curve, whereas the dotted curve represents the response without control.

For *CSMC* controllers, the control parameters are given as follows: (i) 5-sensor case; $\mathbf{Q}$ = diag [10, 10, 10, 80, 0, 0, 0, 0, 100, 10, 10, 110], $\delta = 80$, (ii) 3-sensor case; $\mathbf{Q}$ = diag [10, 10, 10, 80, 0, 0, 0, 0, 100, 10, 10, 110], $\delta = 80$, and (iii) 1-sensor case; $\mathbf{Q}$ = diag.[10, 10, 10, 80, 0, 0, 0, 0, 100, 10, 10, 110], $\delta = 80$. For the observer design for all three cases, we consider $\gamma = S_{\ddot{x}_g \ddot{x}_g} / S_{v_i v_i} = 5$ such that the criterion for the stability robustness is satisfied. The loop transfer functions for *CSMC* controllers are shown in Fig. 5 (b), in which the 5-sensor, 3-sensor and 1-sensor cases are denoted by the solid curve, dashed-dot curve and dashed curve, respectively. J_1

to J_{10} as well as σ_u and $|u(t)|$ for the evaluation model are presented in columns (3), (7) and (11) of Table 3 for 5-sensor, 3-sensor and 1-sensor cases, respectively. For the 5-sensor case using *CSMC* control, the time history of the third-story drift under El Centro earthquake is presented in Fig. 6 (b) by the solid curve, whereas the dotted curve represents the response without control. The time history of the sliding surface S for the 5-sensor case is also plotted in Fig. 6 (c). As observed from Fig. 6 (c), the sliding surface motion $S = 0$ is not maintained because : (i) the feedforward compensation in Eq. (9) has been ignored, and (ii) the estimation of the state, $\mathbf{x}_r$, from an observer is required in the computation of the control command. However, the stability of S is always guaranteed. As observed from Table 3, the control performances for both *LQG* and *CSMC* controllers are remarkable even using only one acceleration sensor on the top floor.

For *CSMC&C* controllers, the parameters for the filter are chosen to be $\mathbf{A}_\eta = -10\,\mathbf{I}_m$ and $\mathbf{B}_\eta = 10\,\mathbf{I}_m$, where m is the number of sensor. The design parameters are given as follows : (i) 5-sensor case; Q_z = diag [10, 10, 10, 0, 0, 0, 0, 0, 10, 10, 10, 20], $\mathbf{Q}_\eta$ = diag [0, 0, 0, 0, 0], $Q_{q_1} = 1$, $R_u = 30$, $R_{\dot{q}_1} = 0.1$, $L_{12} = 0.1$, $L_{22} = -2$, $P_1 = 1$, $P_2 = 1$, $D_2 = 1$ and $\delta = 100$, (ii) 3-sensor case; $\mathbf{Q}_z$ = diag [1, 1, 1, 0, 0, 0, 0, 0, 1, 1, 1, 150], $\mathbf{Q}_\eta$ = diag [0, 0, 0], $Q_{q_1} = 1$, $R_u = 200$, $R_{\dot{q}_1} = 0.1$, $L_{12} = 0.1$, $L_{22} = -2$, , $P_1 = 1$, $P_2 = 1$, $D_2 = 1$ and $\delta = 100$, (iii) 1-sensor case; $\mathbf{Q}_z$ = diag [1, 1, 1, 0, 0, 0, 0, 0, 1, 1, 1, 10], $\mathbf{Q}_\eta = 0$, $Q_{q_1} = 1$, $R_u = 10$, $R_{\dot{q}_1} = 0.1$, $L_{12} = 0.1$, $L_{22} = -2$, , $P_1 = 1$, $P_2 = 1$, $D_2 = 1$ and $\delta = 100$. As in the active mass driver system, a smaller $\mathbf{A}_\eta$ and $\mathbf{B}_\eta$ can satisfy the criterion for stability robustness. The loop transfer functions of *CSMC&C* controllers are plotted in Fig. 5 (c) in which the solid curve, dashed-dot curve and dashed curve denote the loop transfer functions for the 5-sensor, 3-sensor and 1-sensor cases, respectively. J_1 to J_{10} as well as σ_u and $|u(t)|$ for the evaluation model are presented in columns (4), (8) and (12) of Table 3 for 5-sensor, 3-sensor and 1-sensor cases, respectively. For the 5-sensor case using *CSMC&C* control, the time history of the third-story drift under El Centro earthquake is presented in Fig. 6 (d) by the solid curve, whereas the dotted curve represents the response without control. The time history of the sliding surface S for the 5-sensor case is also plotted in Fig. 6 (e). As observed from Fig. 6 (e), the sliding surface motion $S = 0$ is well maintained, since the control command in Eq. (31) always guarantees $\dot{V} \le 0$.

It is observed from Table 3 that the control performances of *CSMC* controllers are comparable to those of *LQG* controllers. Although the performance of *CSMC&C* is slightly worse than *LQG* and *CSMC*; however, it is easier to implement *CSMC&C* controllers because the dimension of the dynamic output feedback equation is smaller.

IV. CONCLUSIONS

The methods of continuous sliding mode control (*CSMC*) and continuous sliding mode control with a compensator (*CSMC&C*) have been applied to two benchmark models. Due to the specific identification scheme used in the benchmark problem in which the state variables are fictitious and the output measurement **y** involves both the control signal and the earthquake excitation, static output feedback controllers are not applicable and therefore the design of *CSMC* and *CSMC&C* controllers becomes more involved. Likewise, the performances of *CSMC* and *CSMC&C* controllers may have been compromised. As a result, an observer is used for *CSMC* controllers, whereas a low-pass filter is introduced for each measurement in *CSMC&C* controllers.

The purpose of introducing filters in *CSMC&C* is to transform the benchmark formulations into strictly proper forms such that the framework of static output feedback can be used. The design procedures for *CSMC&C* involve *LQR* static output feedback such that numerical iterations are required. To obtain a convergent solution, we start with a larger weighting R_u for the control effort u_{eq}, and then reduce R_u gradually. The solution for the previous R_u is used as the initial trial for the next R_u value. Further, the compensator parameters L_{12} and L_{22} were assigned such that not only the compensator system matrix **L** is stable but also the open-loop system of compensator is stable. As a result, the design procedures and computational efforts involved in designing a *CSMC&C* controller is much more involved than that of *CSMC* and *LQG* controllers. However, an advantage of the *CSMC&C* controllers is that the on-line computational effort is reduced because the dimension (i. e., m+2) of filters and compensator is smaller than that of an observer.

The robustness of stability and noise rejection has been presented by plotting the loop transfer function of the controller. To ensure a larger stability margin, the loop transfer function

should be as small as possible in the high frequency range. For this purpose, a trade-off has been made for the selection of the intensity of white noise excitation and measurement noise for *LQG* and *CSMC* methods. For the *CSMC&C* method, the stability margin can be enlarged sufficiently by choosing smaller $\mathbf{A}_\eta$ and $\mathbf{B}_\eta$. Simulation results indicate that the performances of *CSMC* and *CSMC&C* controllers are quite comparable to that of the *LQG* method.

V. ACKNOWLEDGMENT

This paper is supported by the National Science Foundation through Grant No. CMS-96-25616.

VI. REFERENCES

1. V. I. Utkin, *Sliding Modes in Control Optimization*, Springer-Verlag, Berlin, 1992.
2. F. Zhou, and D. G. Fisher, "Continuous Sliding Mode Control", *International J. of Control*, 55(2), 313-327 (1992).
3. J. N. Yang, J. C Wu and A. K. Agrawal, "Sliding Mode Control for Seismic-Excited Linear and Nonlinear Structures", *Technical Report NCEER-94-0017*, National Center for Earthquake Engineering Research, SUNY Buffalo, N. Y., 1994.
4. J. N. Yang, J. C. Wu and A. K. Agrawal, "Sliding Mode Control of Nonlinear and Hysteretic Structures", *ASCE J. of Engrg. Mech.*, 121(12), 1330-1339 (1995).
5. J. N. Yang, J. C. Wu and A. K. Agrawal, "Sliding Mode Control of Seismically Excited Linear Structures", *ASCE J. of Engrg. Mech.*, 121(12), 1386-1390 (1995).
6. M. P. Singh, E. Matheu and L. E. Suarez, "Active and Semi-Active Control of Structures Under Seismic Excitation," *Journal of Earthquake Engineering and Structural Dynamics,* 26(2), 193-213 (1997).
7. J. N. Yang, J. C. Wu, A. M. Reinhorn and M. Riley, "Control of Sliding-Isolated Buildings Using Sliding Mode Control," *ASCE Journal of Structural Engineering*, 122(2), 83-91 (1996).
8. J. N. Yang, J. C., K. Kawashima and S. Unjoh, "Hybrid Control of Seismic-Excited Bridge Structures," *J. Earthquake Engineering and Structural Dynamics*, 24(11), 1437-1451 (1995).

9. J. N. Yang, J. C. Wu and Z. Li, "Control of Seismic-Excited Buildings Using Active Variable Stiffness Systems," *J. of Engrg. Structures*, 18(8), 589-596 (1996).
10. J. N. Yang, J. C. Wu, A. M. Reinhorn, M. Riley, W. E. Schmitendorf and F. Jabbari, "Experimental Verifications of H_∞ and Sliding Mode Control for Seismic-Excited Buildings," *ASCE Journal of Structural Engineering*, 122(1), 69-75 (1996).
11. S. V. Yallapragada and B. S. Heck, "Optimal Control Design for Variable Structure Systems with Fixed Order Compensators," *Proc. of American Control Conference*, 1, 876-880 (1992).
12. J. N. Yang, A. K. Agrawal and J. C. Wu, "Sliding Mode Control of Structures subjected to Seismic Loads," *Proc. of First World Conference on Structural Control*, 1, WA1-13 to WA1-22, USC Publication, Los Angeles (1994).
13. J. N. Yang, J. C. Wu, J. C., A. K. Agrawal and S. Y. Hsu, "Reduced-Order Sliding Mode Control with Compensators for Seismic Response Control," *Proc. of 11th World Conf. on Earthquake Engrg.*, Acapulco, Mexico, Paper No. 273 (1996).
14. B. F. Spencer, S. J. Dyke and H. S. Deoskar, "Benchmark Problems in Structural Control Part I: Active Mass Driver Systems", To appear *in Journal of Earthquake Engineering and Structural Dynamics* (1997).
15. B. F. Spencer, S. J. Dyke and H. S. Deoskar, "Benchmark Problems in Structural Control Part II : Active Tendon System", To appear *in Journal of Earthquake Engineering and Structural Dynamics* (1997).
16. J. C. Wu, "Active Control of Wind-Excited Structures" *Ph.D. Dissertation, University of California, Irvine*, CA, 1996.
17. J. C. Doyle and G. Stein, "Multivariable Feedback Design : Concepts for a Classical/Modern Synthesis", *IEEE Transactions on Automatic Control*, AC-26(1), 4-16 (1981).
18. E. J. Davison, "A Method for Simplifying Linear Dynamic Systems", *IEEE Transactions on Automatic Control*, AC-11(1), 93-101 (1966).
19. W. S. Levine and M. Athans, "On the Determination of the Optimal Constant Output Feedback Gains for Linear Multivariable Systems", *IEEE Transactions on Automatic Control*, AC-15(1), 44-48 (1970).

APPENDIX : Derivations and Design Procedures for Sliding Surface of *CSMC&C*

To confine the response trajectory on the sliding surface, the conditions, $S = 0$ and $\dot{S} = 0$, should be satisfied. Then, it follows from Eq. (28) that

$$q_2 = - P_2^{-1} P_1 \; q_1 \tag{A.1}$$

provided that P_2 is invertible, and

$$\dot{S} = P_1 \; \dot{q}_1 + P_2 \; \dot{q}_2 = 0 \tag{A.2}$$

Substituting Eqs. (A.1), (26) and (27) into Eq. (A.2), one obtains the control force u, denoted by u_{eq} , as

$$u_{eq} = \mathbf{G}\,\eta + H \; q_1 \tag{A.3}$$

in which

$$\mathbf{G} = - (P_2 D_2)^{-1} \; (P_1 N_1 + P_2 N_2) \tag{A.4}$$

$$H = - (P_2 D_2)^{-1} \; [\; P_1 \; (\; L_{11} - L_{12} P_2^{-1} P_1 \;) + P_2 (\; L_{21} - L_{22} P_2^{-1} P_1 \;) \;] \tag{A.5}$$

where u_{eq} is referred to as the equivalent control force, that is the control force needed to confine (or maintain) the system on the sliding surface $S = 0$, once the system trajectory reaches $S = 0$.

Substitution of the equivalent control u_{eq} into the augmented design model, Eq. (22), the closed-loop system of the structure on the sliding surface is given by

$$\dot{\tilde{\mathbf{x}}}_r = \tilde{\mathbf{A}}_r \; \tilde{\mathbf{x}}_r + \tilde{\mathbf{B}}_r \; u_{eq} \tag{A.6}$$

in which the excitation $\tilde{\mathbf{W}}$ has been neglected. Note that in the design of the sliding surface, the external excitation is neglected; however, it is taken into account in the design of the controller. Substitution of q_2 given by Eq. (A.1) into Eq. (27) leads to the compensator dynamics for q_1 on the sliding surface as

$$\dot{q}_1 = (\; L_{11} - L_{12} P_2^{-1} P_1 \;) \; q_1 + N_1 \; \mathbf{y} \tag{A.7}$$

Thus, the entire structure-compensator system on the sliding surface defined by Eqs. (A.6) and (A.7) can be cast into an augmented state equation of strictly proper form with a $(r+m+1)$-dimensional state vector $\overline{\mathbf{Z}}$,

$$\dot{\overline{\mathbf{Z}}} = \overline{\mathbf{A}} \; \overline{\mathbf{Z}} + \overline{\mathbf{B}} \; \overline{u} \tag{A.8}$$

$$\overline{\mathbf{y}} = \overline{\mathbf{C}} \; \overline{\mathbf{Z}} \tag{A.9}$$

in which

$$\bar{\mathbf{Z}}=\begin{bmatrix}\tilde{\mathbf{x}}_r\\ q_1\end{bmatrix};\ \bar{\mathbf{y}}=\begin{bmatrix}\eta\\ q_1\end{bmatrix};\ \bar{\mathbf{A}}=\begin{bmatrix}\tilde{\mathbf{A}}_r & 0\\ 0 & 0\end{bmatrix};\ \bar{\mathbf{B}}=\begin{bmatrix}\tilde{\mathbf{B}}_r & 0\\ 0 & 1\end{bmatrix};\ \bar{u}=\begin{bmatrix}u_{eq}\\ \dot{q}_1\end{bmatrix};\ \bar{\mathbf{C}}=\begin{bmatrix}\tilde{\mathbf{C}}_{yr} & 0\\ 0 & 1\end{bmatrix} \tag{A.10}$$

and Eqs. (A.3) and (A.7) can be combined as

$$\bar{u}=\bar{\mathbf{G}}\ \bar{\mathbf{y}} \tag{A.11}$$

in which

$$\bar{\mathbf{G}}=\begin{bmatrix}\mathbf{G} & H\\ N_1 & L_{11}-L_{12}\,P_2^{-1}\,P_1\end{bmatrix} \tag{A.12}$$

P_1 and P_2 as well as the compensator characteristics will be determined from the augmented system defined by Eqs. (A.8)-(A.9). For the augmented system in Eqs. (A.8)-(A.9) with the static output control in Eq. (A.11), the gain matrix $\bar{\mathbf{G}}$ can be obtained by minimizing a quadratic performance index, Eq. (29). Eq. (29) can be further rearranged into the typical form of

$$J=\mathrm{E}\left\{\int_0^\infty \begin{bmatrix}\bar{\mathbf{Z}}' & \bar{u}'\end{bmatrix}\begin{bmatrix}\bar{\mathbf{Q}} & \bar{\mathbf{S}}\\ \bar{\mathbf{S}}' & \bar{\mathbf{R}}\end{bmatrix}\begin{bmatrix}\bar{\mathbf{Z}}\\ \bar{u}\end{bmatrix}dt\right\} \tag{A.13}$$

in which

$$\bar{\mathbf{Q}}=\begin{bmatrix}\mathbf{C}_{zr}'\mathbf{Q}_z\mathbf{C}_z & 0 & 0\\ 0 & \mathbf{Q}_\eta & 0\\ 0 & 0 & \mathbf{Q}_{q_1}\end{bmatrix};\ \bar{\mathbf{R}}=\begin{bmatrix}\mathbf{D}_z'\mathbf{Q}_z\mathbf{C}_z+\mathbf{R}_u & 0\\ 0 & \mathbf{R}_{\dot{q}_1}\end{bmatrix};\ \bar{\mathbf{S}}=\begin{bmatrix}\mathbf{C}_z'\mathbf{Q}_z\mathbf{D}_z & 0\\ 0 & 0\\ 0 & 0\end{bmatrix} \tag{A.14}$$

As observed from Eq. (A.13), the coupled weighting matrix $\bar{\mathbf{S}}$ between $\bar{\mathbf{Z}}$ and $\bar{u}$ is included in the performance index J. The optimal static output feedback solution by Levine and Athans[19], which does not include the coupled weighting matrix, is generalized and obtined in the following. The gain matrix $\bar{\mathbf{G}}$ in Eq. (A.12) is obtained as

$$\bar{\mathbf{G}}=-\bar{\mathbf{R}}^{-1}(\bar{\mathbf{B}}'\bar{\mathbf{K}}\bar{\mathbf{L}}\bar{\mathbf{C}}'+\bar{\mathbf{S}}'\bar{\mathbf{L}}\bar{\mathbf{C}}')(\bar{\mathbf{C}}\bar{\mathbf{L}}\bar{\mathbf{C}}')^{-1} \tag{A.15}$$

where $\bar{\mathbf{K}}$ and $\bar{\mathbf{L}}$ satisfy the following nonlinear equations

$$\begin{aligned}&\bar{\mathbf{M}}'\bar{\mathbf{K}}+\bar{\mathbf{K}}\bar{\mathbf{M}}+\bar{\mathbf{Q}}+\bar{\mathbf{S}}\bar{\mathbf{G}}\bar{\mathbf{C}}+\bar{\mathbf{C}}'\bar{\mathbf{G}}'\bar{\mathbf{S}}'+\bar{\mathbf{C}}'\bar{\mathbf{G}}'\bar{\mathbf{R}}\bar{\mathbf{G}}\bar{\mathbf{C}}=0\\ &\mathbf{I}+\bar{\mathbf{M}}\bar{\mathbf{L}}+\bar{\mathbf{L}}\bar{\mathbf{M}}'=0\\ &\bar{\mathbf{M}}=\bar{\mathbf{A}}+\bar{\mathbf{B}}\bar{\mathbf{G}}\bar{\mathbf{C}}\end{aligned} \tag{A.16}$$

Note that Eqs. (A.15)-(A.16) can be solved for $\overline{\mathbf{G}}$, $\overline{\mathbf{L}}$, $\overline{\mathbf{M}}$, $\overline{\mathbf{K}}$ iteratively. Once $\overline{\mathbf{G}}$ is obtained, the following procedures can be used to compute matrices $\mathbf{N}_1$, $\mathbf{N}_2$, L_{11}, L_{12}, L_{21}, L_{22} and D_2 of the compensator and P_1, P_2 of the sliding surface: (i) $\mathbf{G}$, H, N_1 and $(L_{11} - L_{12} P_2^{-1} P_1)$ can be determined from Eq. (A.12); (ii) with $\mathbf{G}$ obtained in (i), N_2 can be determined from Eq. (A.4) by assigning nonsingular P_2, D_2 and any P_1; (iii) From Eq. (A.5) and H obtained above, L_{21} can be determined by assigning appropriate L_{22}; (iv) Since $(L_{11} - L_{12} P_2^{-1} P_1)$ is known, L_{11} can be determined by assigning appropriate L_{12}. L_{12} and L_{22} are chosen to guarantee the stability of the open-loop compensator equation. From a conservative point of view, a stable open-loop compensator equation is preferable in case the control force is saturated due to the limitation of the actuator capacity (see Yang et al[12]).

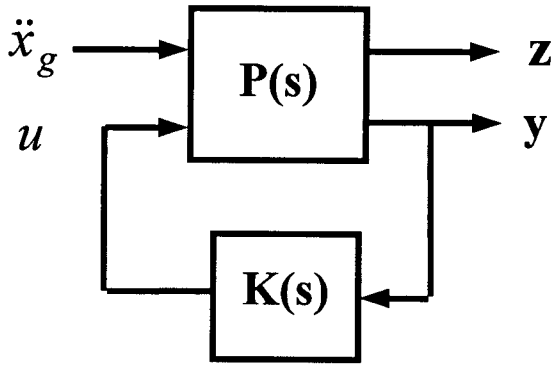

Fig. 1 : Control Diagram for Benchmark Systems

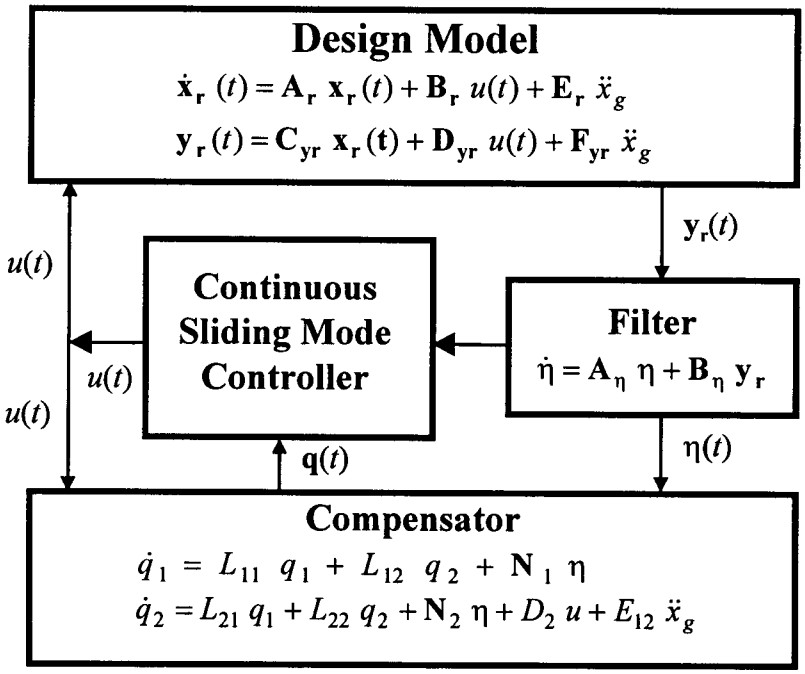

Fig. 2 : Block Diagram of Continuous Sliding Mode Control with Compensator (*CSMC&C*)

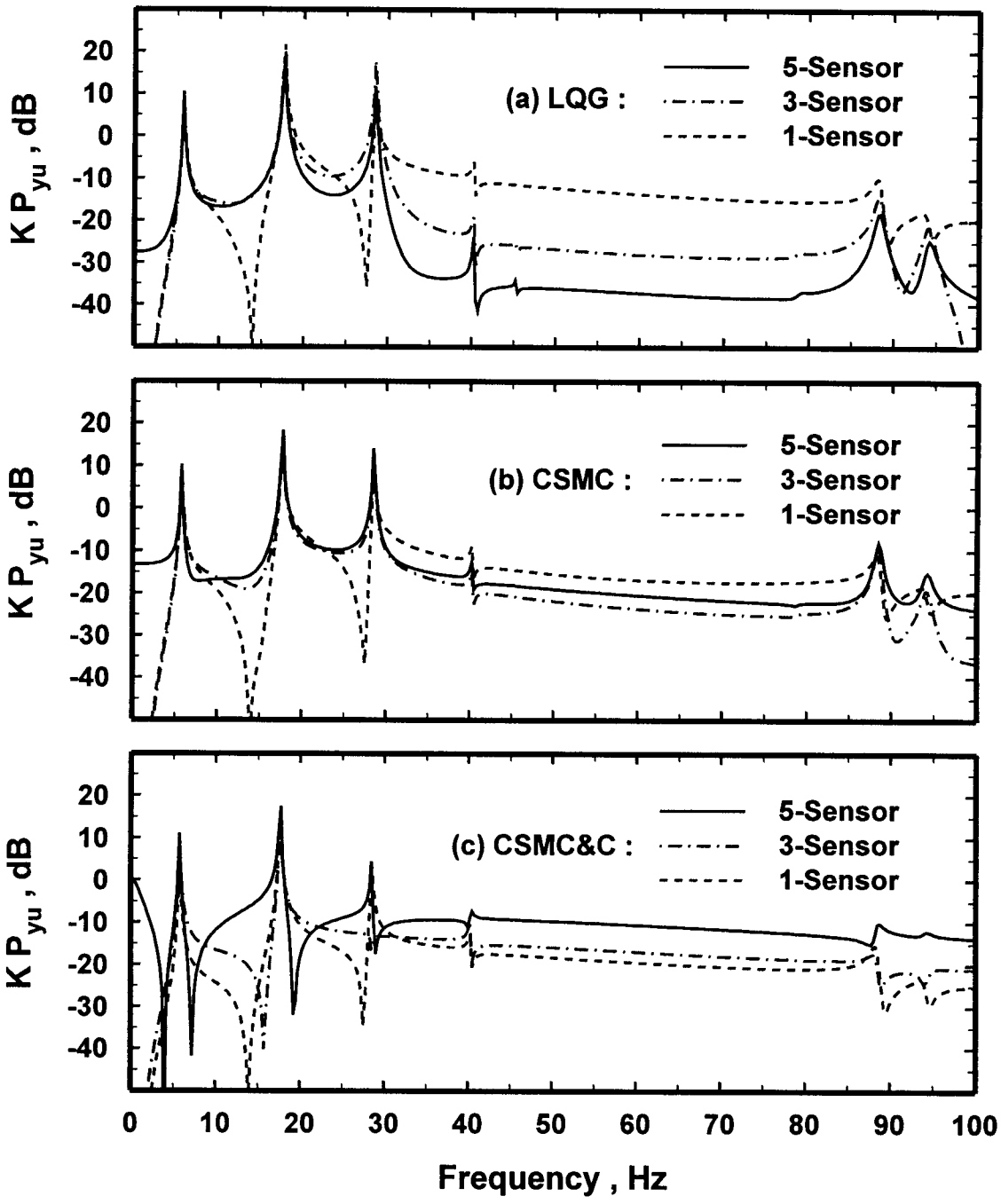

Fig. 3 : Loop Transfer Functions for Active Mass Driver System for ;
(a) LQG, (b) CSMC, and (c) CSMC&C Methods

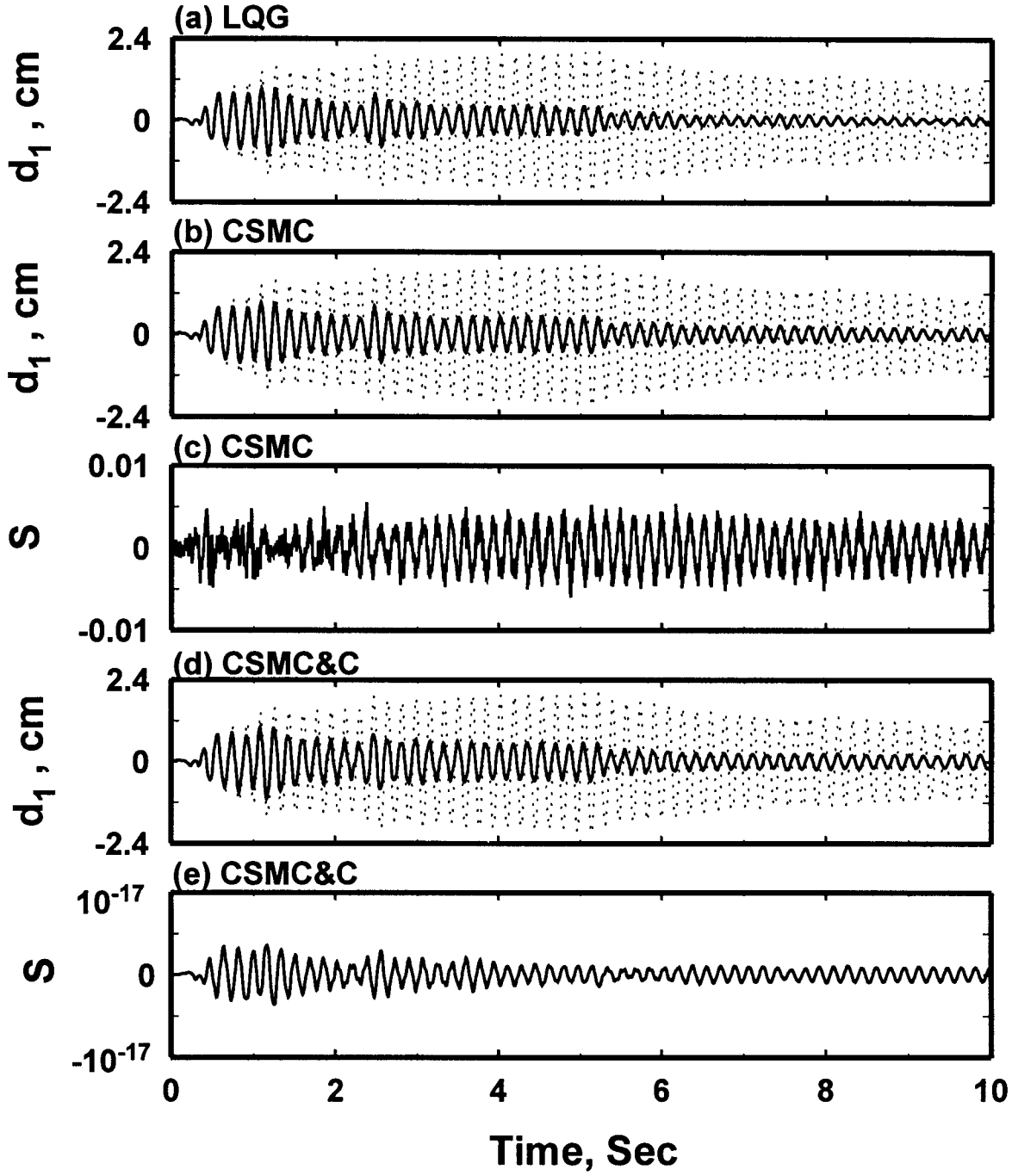

Fig. 4 : Time Histories of First-Story Drift and Sliding Surface for Active Mass Driver System under El Centro Earthquake (5-Sensor Case) Using LQG, CSMC and CSMC&C Controllers

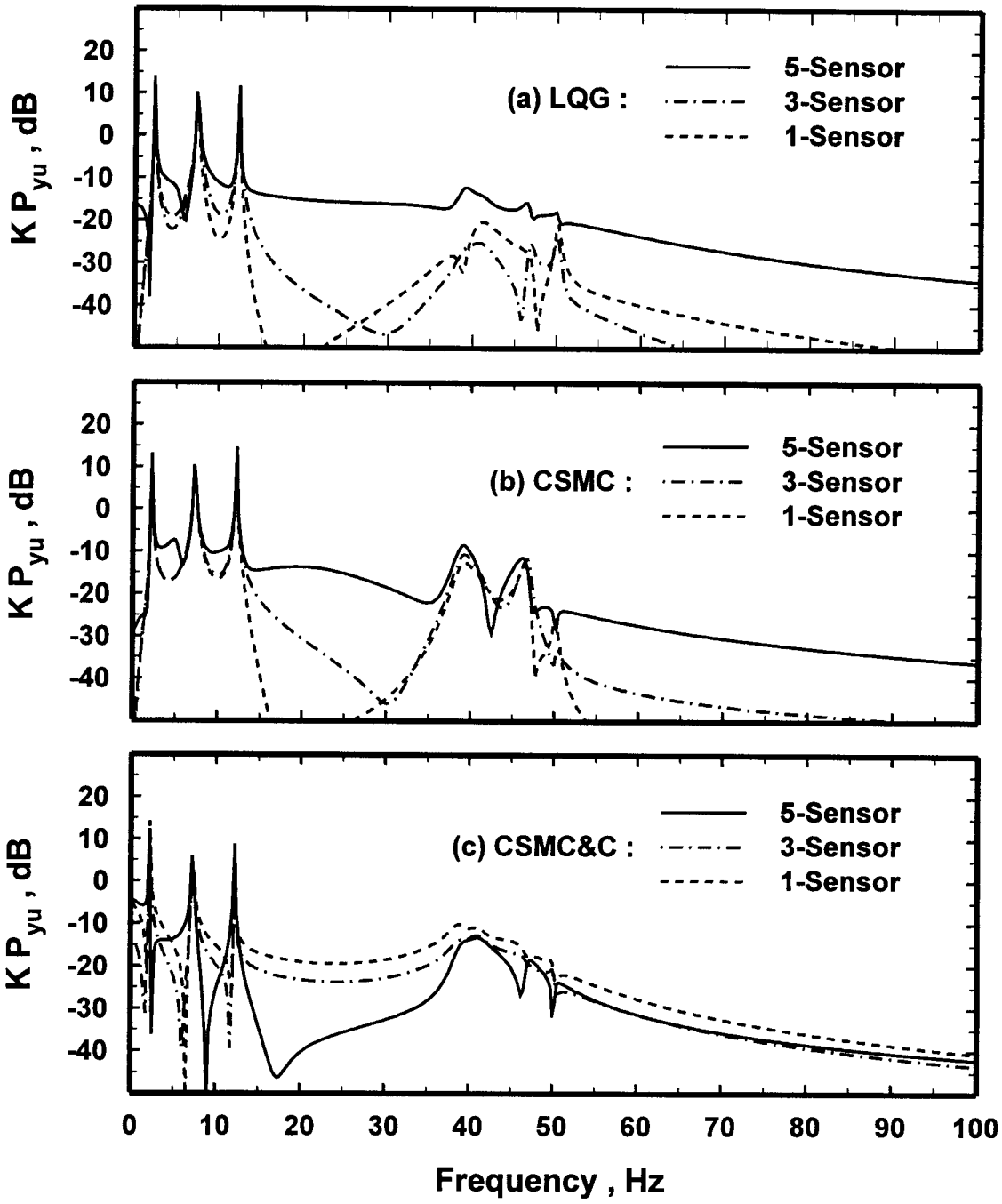

Fig. 5 : Loop Transfer Functions for Active Tendon System for ;
(a) LQG, (b) CSMC, and (c) CSMC&C Methods

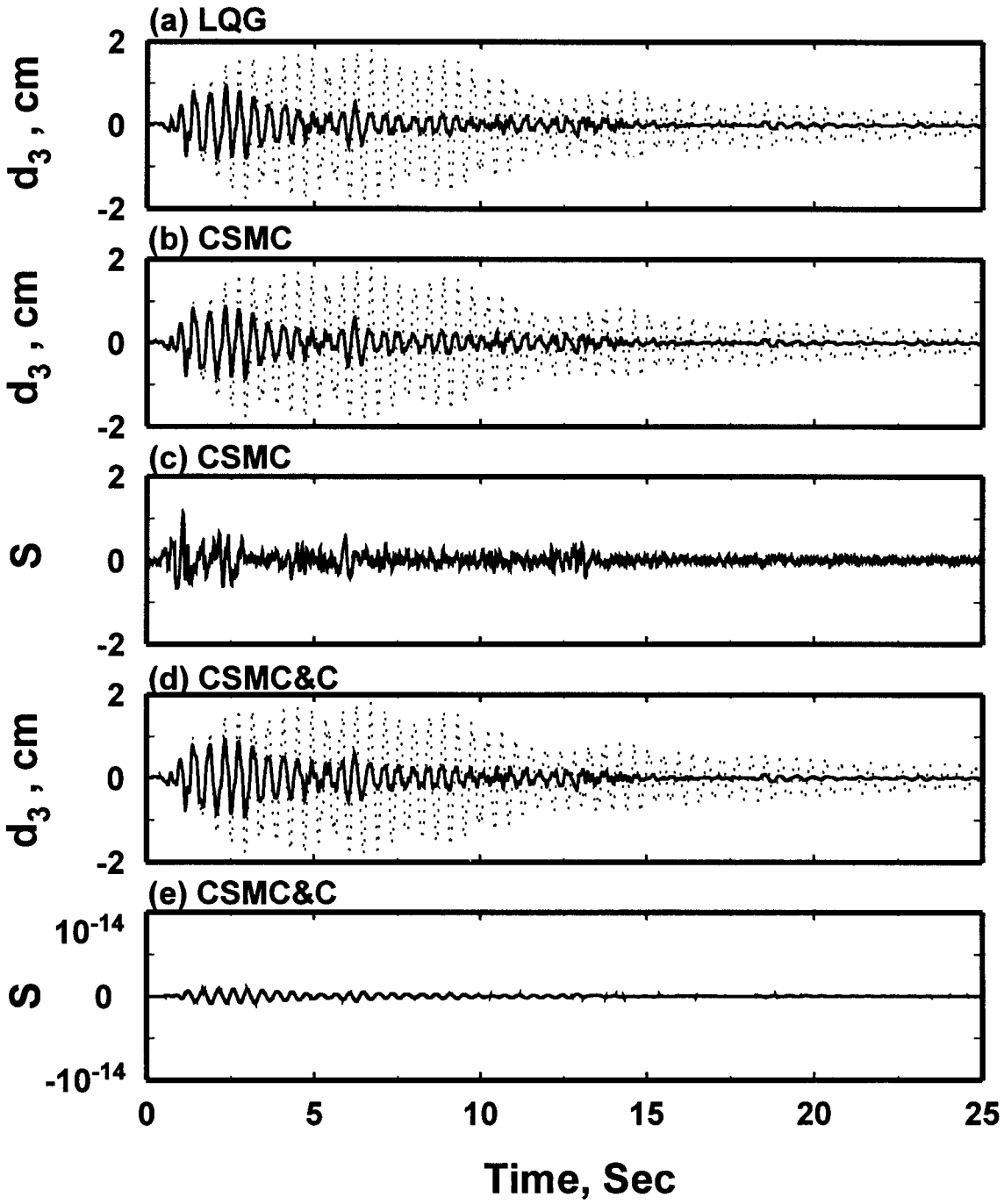

Fig. 6 : Time Histories of Third-Story Drift and Sliding Surface for Active Tendon System under El Centro Earthquake (5-Sensor Case) Using LQG, CSMC and CSMC&C Controllers

Table 1 : Structural Response Quanitites with Zero Control Input

Active Mass Driver System										
	El Centro			Hachinohe			Artificial Earthquake			
(1) Quantities	(2) Story			(2) Story			(4) Quantities	(5) Story		
	1	*2*	*3*	*1*	*2*	*3*		*1*	*2*	*3*
x_i (cm)	2.09	3.29	3.44	0.96	1.52	1.66	σ_{x_i} (cm)	0.75	1.21	1.28
d_i (cm)	2.09	1.21	0.27	0.96	0.59	0.15	σ_{d_i} (cm)	0.75	0.45	0.08
$\ddot{x}_{ai}$ (g)	3.34	4.62	5.05	1.85	2.17	2.69	$\sigma_{\ddot{x}_{ai}}$ (g)	1.04	1.64	1.75
x_m (cm)	0.25			0.13			σ_{x_m} (cm)	0.09		
$\dot{x}_m$ (cm/s)	10.32			4.84			$\sigma_{\dot{x}_m}$ (cm/s)	3.38		
$\ddot{x}_{am}$ (g)	5.43			2.94			$\sigma_{\ddot{x}_{am}}$ (kN)	1.87		
Active Tendon System										
	El Centro			Hachinohe			Artificial Earthquake			
(1) Quantities	(2) Story			(2) Story			(4) Quantities	(5) Story		
	1	*2*	*3*	*1*	*2*	*3*		*1*	*2*	*3*
x_i (cm)	2.03	4.97	6.57	1.19	2.95	3.85	σ_{x_i} (cm)	0.70	1.80	2.40
d_i (cm)	2.03	3.09	1.81	1.19	1.77	0.95	σ_{d_i} (cm)	0.70	1.11	0.60
$\ddot{x}_{ai}$ (g)	1.08	1.18	1.57	0.43	0.67	0.78	$\sigma_{\ddot{x}_{ai}}$ (g)	0.15	0.37	0.49
x_m (cm)	0.060			0.035			σ_{x_m} (cm)	0.020		
$\dot{x}_m$ (cm/s)	1.072			0.490			$\sigma_{\dot{x}_m}$ (cm/s)	0.290		
f (kN)	23.08			13.54			σ_f (kN)	7.90		

Table 2 : Comparison of Evaluation Criteria for *LQG*, *CSMC*, and *CSMC&C* Controllers for Active Mass Driver System

Quantities	*LQG*		*CSMC*		*CSMC&C*	
Five-Sensor Case, $\mathbf{y}_r = [x_m, \ddot{x}_{a1}, \ddot{x}_{a2}, \ddot{x}_{a3}, f]'$						
(1)	(2)		(3)		(4)	
J_1	0.1878		0.1979		0.2114	
J_2	0.2846		0.2936		0.3183	
J_3	0.8444		0.8221		0.7783	
J_4	0.8259		0.8042		0.7560	
J_5	0.8327		0.7775		0.6443	
σ_u (volts)	0.2710		0.2668		0.2637	
$\sigma_{\ddot{x}_{am}}$ (g)	1.4905		1.3917		1.1534	
σ_{x_m} (cm)	1.1062		1.0770		1.0196	
	El Centro	Hachinohe	El Centro	Hachinohe	El Centro	Hachinohe
J_6	0.3083	0.3779	0.3077	0.3738	0.3275	0.3757
J_7	0.4725	0.6616	0.4730	0.6674	0.6201	0.6287
J_8	1.2479	1.6240	1.2338	1.6832	1.1971	1.7292
J_9	1.2098	1.4811	1.2183	1.4903	1.2097	1.4550
J_{10}	1.1078	1.6491	1.0749	1.5673	1.1071	1.2821
max $\lvert u \rvert$ (volts)	1.1601	0.7539	1.1481	0.7818	1.1612	0.8087
max $\lvert \ddot{x}_{am} \rvert$ (g)	5.5942	4.2546	5.4282	4.0435	5.5908	3.3077
max $\lvert x_m \rvert$ (cm)	4.2056	2.6958	4.1578	2.7941	4.0343	2.8705
Three-Sensor Case, $\mathbf{y}_r = [\ddot{x}_{a1}, \ddot{x}_{a2}, \ddot{x}_{a3}]'$						
(5)	(6)		(7)		(8)	
J_1	0.1943		0.1963		0.1948	
J_2	0.2956		0.2956		0.2939	
J_3	0.8126		0.8110		0.8286	
J_4	0.7984		0.7970		0.7945	
J_5	0.8287		0.8004		0.7409	
σ_u (volts)	0.2567		0.2599		0.2742	
$\sigma_{\ddot{x}_{am}}$ (g)	1.4834		1.4327		1.3261	
σ_{x_m} (cm)	1.0645		1.0625		1.0855	
	El Centro	Hachinohe	El Centro	Hachinohe	El Centro	Hachinohe
J_6	0.3164	0.3818	0.3112	0.3760	0.3068	0.3700
J_7	0.4888	0.6691	0.4888	0.6695	0.5559	0.6269
J_8	1.1783	1.5022	1.2051	1.5819	1.2415	1.8663
J_9	1.1608	1.4376	1.1870	1.4060	1.2345	1.5739
J_{10}	1.1026	1.7515	1.1204	1.4647	1.1817	1.5217
max $\lvert u \rvert$ (volts)	1.0989	0.7071	1.1267	0.7350	1.1906	0.8686
max $\lvert \ddot{x}_{am} \rvert$ (g)	5.5680	3.5189	5.6581	3.7790	5.9677	3.9260
max $\lvert x_m \rvert$ (cm)	3.9710	2.4937	4.0613	2.6260	4.1838	3.0981
One-Sensor Case, $\mathbf{y}_r = [\ddot{x}_{a3}]$						
(9)	(10)		(11)		(12)	
J_1	0.2112		0.2114		0.2661	
J_2	0.3234		0.3235		0.4093	
J_3	0.7696		0.7650		0.5490	
J_4	0.7600		0.7524		0.5428	
J_5	0.7805		0.7677		0.5309	
σ_u (volts)	0.2473		0.2454		0.1710	
$\sigma_{\ddot{x}_{am}}$ (g)	1.3971		1.3741		0.9503	
σ_{x_m} (cm)	1.0082		1.0022		0.7192	
	El Centro	Hachinohe	El Centro	Hachinohe	El Centro	Hachinohe
J_6	0.3196	0.3844	0.3167	0.3784	0.3739	0.4179
J_7	0.4957	0.6915	0.5168	0.6824	0.7188	0.7001
J_8	1.1451	1.3643	1.1360	1.4741	0.6983	0.9366
J_9	1.1442	1.5644	1.1306	1.3974	0.7241	0.9154
J_{10}	1.1706	1.8799	1.1817	1.4123	0.8675	0.9064
max $\lvert u \rvert$ (volts)	1.0638	0.6517	1.0607	0.6844	0.6984	0.4405
max $\lvert \ddot{x}_{am} \rvert$ (g)	5.9118	4.8503	5.9677	3.6438	4.3806	2.3386
max $\lvert x_m \rvert$ (cm)	3.8590	2.2647	3.8283	2.4469	2.3531	1.5548

Table 3 : Comparison of Evaluation Criteria for *LQG*, *CSMC*, and *CSMC&C* Controllers for Active Tendon System

Quantities	*LQG*		*CSMC*		*CSMC&C*	
Five-Sensor Case, $\mathbf{y}_r = [x_p, \ddot{x}_{a1}, \ddot{x}_{a2}, \ddot{x}_{a3}, f]'$						
(1)	(2)		(3)		(4)	
J_1	0.1646		0.1572		0.1727	
J_2	0.3472		0.3387		0.3669	
J_3	0.0329		0.0308		0.0317	
J_4	0.0343		0.0328		0.0307	
J_5	0.0089		0.0095		0.0097	
σ_u (volts)	0.5978		0.5780		0.5811	
σ_f (kN)	2.5703		2.7360		2.7969	
σ_{x_p} (cm)	0.0771		0.0721		0.0743	
	El Centro	Hachinohe	El Centro	Hachinohe	El Centro	Hachinohe
J_6	0.2506	0.3223	0.2421	0.3157	0.2583	0.3245
J_7	0.5252	0.8514	0.4942	0.8437	0.4974	0.8097
J_8	0.0491	0.0662	0.0463	0.0674	0.0520	0.0611
J_9	0.0539	0.0677	0.0594	0.0729	0.0431	0.0549
J_{10}	0.0350	0.0269	0.0373	0.0295	0.0382	0.0266
max $\|u\|$ (volts)	2.4737	1.9540	2.4188	2.0424	2.6109	1.8224
max $\|f\|$ (kN)	10.1196	7.7831	10.7916	8.5367	11.0252	7.6821
max $\|x_p\|$ (cm)	0.3166	0.2502	0.2989	0.2548	0.3355	0.2311
Three-Sensor Case, $\mathbf{y}_r = [\ddot{x}_{a1}, \ddot{x}_{a2}, \ddot{x}_{a3}]'$					$\mathbf{y}_r = [x_p, \ddot{x}_{a3}, f]'$	
(5)	(6)		(7)		(8)	
J_1	0.1681		0.1568		0.1831	
J_2	0.3545		0.3377		0.3802	
J_3	0.0328		0.0312		0.0367	
J_4	0.0341		0.0331		0.0370	
J_5	0.0091		0.0094		0.0090	
σ_u (volts)	0.5948		0.5846		0.6495	
σ_f (kN)	2.6187		2.7268		2.6008	
σ_{x_p} (cm)	0.0768		0.0730		0.0858	
	El Centro	Hachinohe	El Centro	Hachinohe	El Centro	Hachinohe
J_6	0.2559	0.3276	0.2408	0.3166	0.2705	0.3333
J_7	0.5316	0.8603	0.4935	0.8438	0.5522	0.8126
J_8	0.0495	0.0606	0.0468	0.0675	0.0559	0.0631
J_9	0.0515	0.0666	0.0602	0.0737	0.0496	0.0610
J_{10}	0.0354	0.0271	0.0375	0.0294	0.0352	0.0242
max $\|u\|$ (volts)	2.4669	1.7905	2.4220	2.0457	2.7256	1.8084
max $\|f\|$ (kN)	10.2325	7.8390	10.8343	8.4854	10.1765	6.9796
max $\|x_p\|$ (cm)	0.3196	0.2292	0.3015	0.2553	0.3606	0.2387
One-Sensor Case, $\mathbf{y}_r = [\ddot{x}_{a3}]$					$\mathbf{y}_r = [f]$	
(9)	(10)		(11)		(12)	
J_1	0.1620		0.1575		0.1905	
J_2	0.3409		0.3390		0.3927	
J_3	0.0347		0.0312		0.0394	
J_4	0.0362		0.0330		0.0398	
J_5	0.0086		0.0094		0.0090	
σ_u (volts)	0.6297		0.5848		0.6930	
σ_f (kN)	2.4967		2.7269		2.5927	
σ_{x_p} (cm)	0.0812		0.0731		0.0922	
	El Centro	Hachinohe	El Centro	Hachinohe	El Centro	Hachinohe
J_6	0.2497	0.3256	0.2404	0.3190	0.2798	0.3367
J_7	0.5188	0.8578	0.4888	0.8357	0.5748	0.8162
J_8	0.0531	0.0640	0.0473	0.0666	0.0588	0.0640
J_9	0.0558	0.0717	0.0563	0.0715	0.0530	0.0648
J_{10}	0.0346	0.0273	0.0373	0.0293	0.0354	0.0233
max $\|u\|$ (volts)	2.6677	1.8869	2.3976	2.0157	2.8488	1.8233
max $\|f\|$ (kN)	10.0112	7.9026	10.7788	8.4632	10.2429	6.7449
max $\|x_p\|$ (cm)	0.3426	0.2421	0.3049	0.2516	0.3795	0.2421